Integration of a Particle-Particle-Particle-Mesh Algorithm with the Ensemble Monte Carlo Method for the Simulation of Ultra-Small Semiconductor Devices

Carl J. Wordelman, *Member, IEEE,* and Umberto Ravaioli, *Senior Member, IEEE*

***Abstract*—A particle-particle-particle-mesh (P3M) algorithm is integrated with the ensemble Monte Carlo (EMC) method for the treatment of carrier-impurity (c-i) and carrier-carrier (c-c) effects in semiconductor device simulation. Ionized impurities and charge carriers are treated granularly as opposed to the normal continuum methods and c-i and c-c interactions are calculated in three dimensions. The combined P3M-EMC method follows the approach of Hockney, but is modified to treat nonuniform rectilinear meshes with arbitrary boundary conditions. Bulk mobility results are obtained for a three-dimensional (3-D) resistor and are compared with previously reported experimental and numerical results.**

***Index Terms*—Charge carrier processes, molecular dynamics, Monte Carlo methods, particle collisions, particle scattering.**

I. Introduction

THE CONTINUED scaling of CMOS integrated circuits is expected to lead to nano-scale devices. For instance, the SIA road map calls for CMOS transistors with channel lengths of 50 nm by the year 2012 [1]. For traditional device designs and scaling techniques, this will result in transistors having on the order of a hundred impurities in the channel [2]. Impurities at such low numbers would not be well treated in semiconductor device simulation using today's approaches based on smooth impurity profiles. Instead, impurity atoms, and charge carriers will need to be integrated into device simulation individually and methods will need to accurately account for their interaction on an individual basis. In today's devices, high doping concentrations in the contact regions already call for careful treatment of carrier-impurity (c-i) and carrier-carrier (c-c) interactions [3]. For example, granular impurity effects result in lowering n-MOSFET threshold voltages [2], and Monte Carlo simulations including c-c scattering rates predict an increase in the number of hot carriers near MOSFET drains at low temperature [4]. For all of these reasons, improved methods to treat granular effects including the location of impurities and the nature of c-i and c-c interactions have become important.

Manuscript received February 19, 1999; revised August 17, 1999. This work was supported by Semiconductor Research Corporation under Contract 98-SJ-406, the National Science Foundation under Grant ECS 95-09751, and Los Alamos National Laboratory. The review of this paper was arranged by Editor A. H. Marshak.

The authors are with Beckman Institute, University of Illinois at Urbana-Champaign, Urbana, IL 61801 USA (e-mail: ravaioli@uiuc.edu).

Publisher Item Identifier S 0018-9383(00)00696-1.

In the traditional ensemble Monte Carlo (EMC) method, both impurities and carriers are treated as a continuum. The locations of impurities are represented in terms of smooth impurity profiles on a mesh, while the location of carriers are treated precisely, but are smoothly assigned to the mesh using a charge association technique. Coulomb interactions are separated into two types: long-range "mesh" interactions included by solving the Poisson equation and short-range "scattering" interactions included with a screening model and scattering rates.

Scattering rates allow for approximate treatment of c-i and c-c interactions within two-dimensional (2-D) Monte Carlo simulations, but have several disadvantages when used in this context. First, c-i scattering rates are normally based on a two-body model which ignores multi-ion contributions to the scattering potential [5]. Second, c-c scattering rates must be updated during the simulation to account for the local dependence of the distribution function and screening length [6]. Finally, both c-i and c-c scattering rates treat interactions as localized instantaneous events rather than interactions extended in space and time [7].

An alternative to using scattering rates for c-i and c-c interactions is to calculate the short-range forces directly and combine them with the long-range forces found with the mesh. The general combination of direct forces and mesh forces has been studied for ionic and cosmological systems and a number of techniques have been developed. One set of early approaches called particle-particle-particle-mesh (P3M) algorithms were developed by Hockney [8].

In this paper, we treat granular effects in semiconductor devices by integrating a P3M algorithm with the EMC method. The combined P3M-EMC method treats impurities discretely and locates them precisely in the simulation domain. In place of c-i and c-c scattering rates, the actual interparticle forces are calculated and approximate screening behavior of the interacting particles is implicitly accounted for by the net force evaluation. For the case of c-c interactions, the method requires a realistic carrier ensemble size within its domain of use, but can address the true three dimensional (3-D) and granular nature of ultra-small devices with moderate variation to the standard EMC method. The possibility of this approach was suggested by Pacelli [9], and an alternative approach using a short-range correction of the mesh forces has been implemented by Gross *et al.* [3].

0018–9383/00$10.00 © 2000 IEEE

This paper is organized as follows. P3M algorithms are described in Section II including a detailed description of the components of the Coulomb force, a discussion of the so-called reference force which is responsible for smoothing between the short- and long-range domains, and details concerning how the P3M algorithms may be modified to treat nonuniform rectilinear meshes with arbitrary boundary conditions. The modified P3M scheme is verified with Coulomb's law using uniform and nonuniform meshes in Section III. In Section IV, the combined P3M-EMC method and details concerning its implementation are presented. Also in this section, spatial and temporal limitations are evaluated for the accurate simulation of plasma oscillations and simulation results for bulk mobility are obtained for comparison with previously reported experimental and numerical results.

II. P3M ALGORITHMS

Particle–particle-particle-mesh (P3M) algorithms [8] are a class of hybrid algorithms designed to treat correlated systems with long-range forces and allow for a large ensemble size. The essence of P3M algorithms is to express the interparticle force as the sum of a short-range part calculated by a direct particle-particle force summation and a long-range part approximated by the particle-mesh force calculation.

A. P3M Force Components

Using the notation of Hockney [8], the total force on a particle i may be written as

$$F_i = \sum_{j \neq i} F_{ij}^{coul} + F_i^{ext}. \tag{1}$$

F_i^{ext} represents the external field or boundary effects of the global Poisson solution. F_{ij}^{coul} is the force of particle j on particle i given by Coulomb's law as

$$F_{ij}^{coul} = \frac{q_i q_j}{4\pi\epsilon} \frac{(r_i - r_j)}{|r_i - r_j|^3} \tag{2}$$

where q_i and q_j are particle charges and r_i and r_j are particle positions.

In a P3M algorithm, the total force on particle i is split into two sums

$$F_i = \sum_{\substack{j \neq i \\ r_j \in \Omega_i^{sr}}} F_{ij}^{sr} + \sum_{\substack{j \neq i \\ r_j \in \Omega}} F_{ij}^{m}. \tag{3}$$

The first sum represents the direct forces of particles j on particle i within the short-range domain (Ω_i^{sr}), while the second sum represents the mesh forces of particles j on particle i over the global problem domain (Ω) as well as the effect of material boundaries and boundary conditions on particle i. F_{ij}^{sr} is the short-range particle force of particle j on particle i, and F_{ij}^{m} is the long-range mesh force of particle j on particle i. The short-range Coulomb force can be further defined as

$$F_{ij}^{sr} = F_{ij}^{coul} - R_{ij} \tag{4}$$

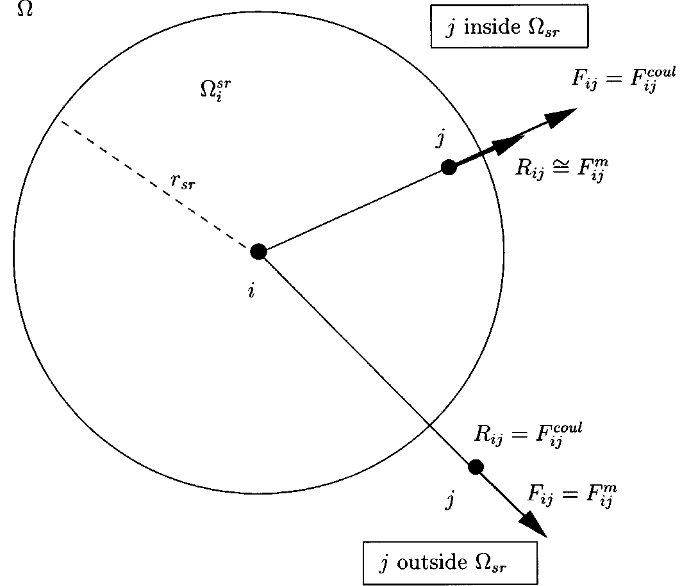

Fig. 1. Diagram of the component forces in the P3M algorithm of particle j on particle i for j inside and outside the short-range domain where F_{ij} is the total force, F_{ij}^{sr} is the short-range force, F_{ij}^{m} is the mesh force, and R_{ij} is the reference force. Ω_i^{sr} is the short-range domain of radius r_{sr} and Ω is the global problem domain which includes Ω_i^{sr}.

where F_{ij}^{coul} is given by (2) and R_{ij} is called the reference force [8].

B. Reference Force

The reference force, R_{ij} in (4), is needed to avoid double counting of the short-range force due to the overlapping domains in (3). In Fig. 1, the reference force can be seen to be equal to the mesh force inside the short-range domain and equal to the Coulomb force outside the short-range domain.

In order to incorporate the effects of material boundaries and boundary conditions, the reference force would be found most precisely in the short-range domain by associating particle j with the particle-mesh and calculating the resulting force on particle i with $F_i^{ext} = 0$. Since such a procedure would be required for each particle, it is obviously too costly for reasonable ensemble sizes and defeats the purpose of the P3M algorithm. Instead, it is desirable to use an approximation for this force which minimizes the effects of the transition error in going from the long-range domain to the short-range domain. One approach developed in [3] is to choose a particular orientation of approaching particles relative to the mesh and find a radial approximation to the reference force. This method is straightforward and computationally efficient per particle for a fixed uniform mesh, but it is not easily adaptable to nonuniform meshes where the mesh force is not isotropic (see force diagram results in Section III).

For the case of nonuniform rectilinear meshes which are often employed in EMC device simulation, we introduce a modification of the original approach to the transition error posed in [8]. In this approach, smoothing of the total interparticle force between the long- and short-range domains can be thought of as

ascribing a finite size to particle i. In particular, Hockney indicates that a sphere with uniformly decreasing density profile, $S(r)$, is a good choice for smoothing in three dimensions.

$$S(r) = \begin{cases} \frac{48}{\pi r_{sr}^4}(r_{sr}/2 - r) & r \le r_{sr}/2 \\ 0 & r > r_{sr}/2. \end{cases} \quad (5)$$

A comparison of the density profile above to that of a uniformly charged sphere and that of a sphere with a Gaussian distribution shows that the expression in (5) produces marginally better accuracy in 3-D schemes for a given cutoff radius r_{sr}. The reference force can be obtained using the definition

$$\begin{aligned} R(r) &= \boldsymbol{R}(\boldsymbol{x}) \cdot \hat{\boldsymbol{r}} \\ &= \frac{\hat{\boldsymbol{r}}}{4\pi\epsilon} \int d\boldsymbol{x}' \int d\boldsymbol{x}'' \\ &\quad \cdot S(x'')S(x' - x'') \frac{(\boldsymbol{x}' - \boldsymbol{x}'')}{|\boldsymbol{x}' - \boldsymbol{x}''|^3}. \end{aligned} \quad (6)$$

When applied to the density profile in (5), one gets (7), shown at the bottom of the page, where

$$\xi = \frac{2r}{r_{sr}}. \quad (8)$$

Hockney advocates precalculating the short-range force, $F_{ij}^{sr}(r)$, in (4) including the reference force above for a fixed uniform mesh and interpolating it at the interaction radius, r.

C. Extension of P3M Algorithms to Nonuniform Meshes

It is important to extend the P3M algorithm to nonuniform meshes for the purpose of semiconductor device simulation since practical device applications involve rapidly varying doping profiles and narrow conducting channels which need to be adequately resolved. Since the mesh force from the solution to the Poisson equation is a good approximation within about two mesh spaces, we modify the P3M algorithm by locally choosing r_{sr} as the shortest distance which spans two mesh cells in each direction of every dimension of the mesh at charge i (see Fig. 2). Using (7), the ξ-dependent portion of the reference force in (6) can be interpolated as a function of ξ in the range $0 < \xi < 2$ and used with r_{sr} to find the reference force.

This modification avoids unnecessary particle-particle force calculations where the particle-mesh (PM) force estimates are adequate for nonuniform rectilinear meshes and would work seamlessly if adaptive meshes were used for the global PM calculation. It should be noted that uncontrolled cost of the particle-particle calculation in the P3M algorithm is a problem in general and this issue may warrant investigation using alternate methods such as the nested-grid particle mesh (NGPM) method [10], the "mesh-refined" P3M algorithm [11] and other N-body methods such as tree codes which can better treat high carrier or impurity densities and low mesh resolution.

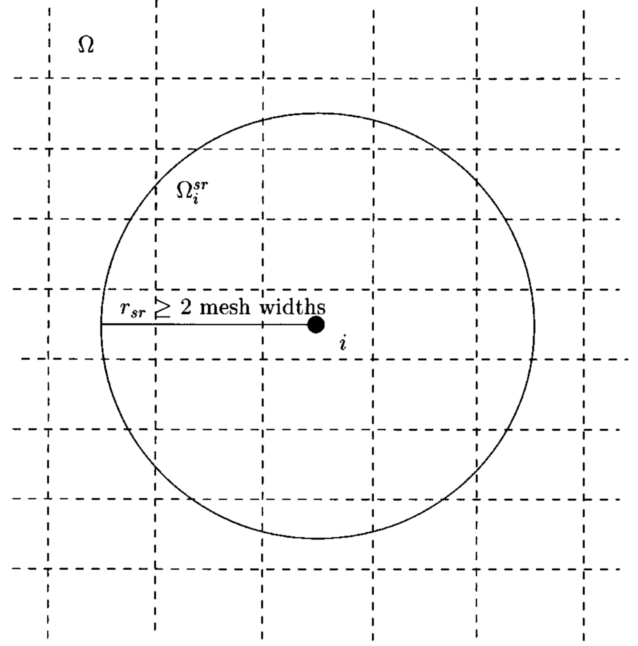

Fig. 2. Diagram of the choice for r_{sr} as the minimum distance which spans a fixed number of mesh cells (we choose 2) in each direction of every dimension of the mesh.

III. Verifying the P3M Implementation with Coulomb's Law

The modification of the P3M algorithm introduced in Section III may be verified and the smoothing of the total interparticle force may be investigated by calculating the force for interacting charges and comparing with Coulomb's law [8]. A pair of charges, $q_i = q_j = e$, are placed in a uniform cube of silicon ($\epsilon_r = 11.8$) with side length 1000 nm. The position of charge i is fixed near the center of the cube, while charge j is moved from 0 to 100 nm from charge i. Note that the separation of the charges is modest with respect to the extent of the mesh and that charge-neutral boundary conditions are used at all edge planes. The magnitude of the mesh force, $|F_{ij}|/q_i$, is

$$R_{ij}(r) = \frac{q_i q_j}{4\pi\epsilon} \times \begin{cases} \frac{1}{35 r_{sr}^2}(224\xi - 224\xi^3 + 70\xi^4 + 48\xi^5 - 21\xi^6) & 0 \le r \le r_{sr}/2 \\ \frac{1}{35 r_{sr}^2}\left(\frac{12}{\xi^2} - 224 + 896\xi - 840\xi^2 + 224\xi^3 + 70\xi^4 - 48\xi^5 + 7\xi^6\right) & r_{sr}/2 \le r \le r_{sr} \\ \frac{1}{r^2} & r > r_{sr} \end{cases} \quad (7)$$

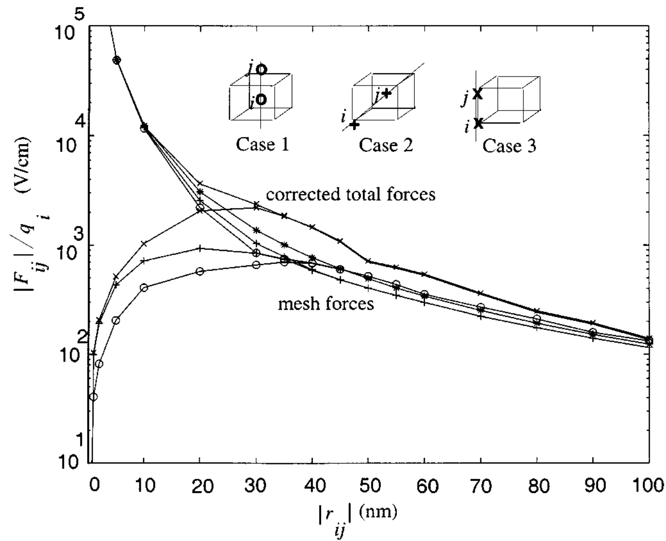

Fig. 3. Force diagram for Si using a uniform mesh is shown for three orientations of separated charges relative to the mesh (o, +, and × as shown above) and with the results of Coulomb's law (∗). The lower lines denote the mesh forces, while the upper lines denote the corrected total forces.

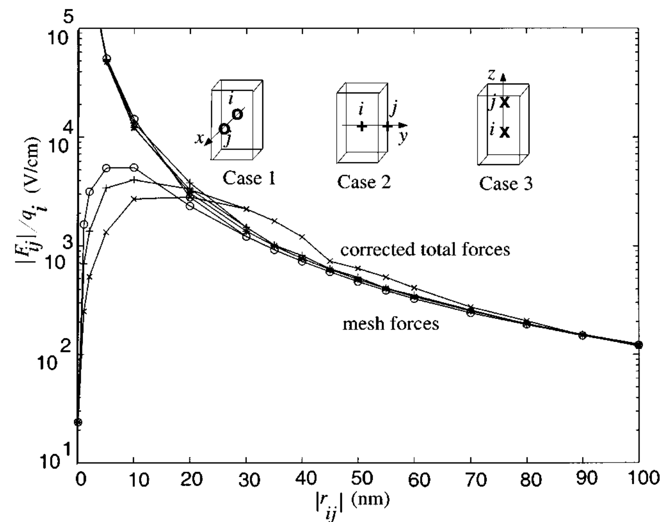

Fig. 4. Force diagram for Si using a nonuniform mesh is shown for the moved charge, j, placed along each axis (o, +, and × as shown above) and compared with the results of Coulomb's law (∗). The lower lines denote the mesh forces while the upper lines denote the corrected total forces.

found using a uniform rectilinear mesh $(41 \times 41 \times 41)$ and the results are compared with the magnitude of the Coulomb force in Fig. 2.

To emphasize the dependence of the mesh force on the location of the charges, three orientations of the charges with respect to the mesh are considered and the interparticle force is calculated for each (see Fig. 3). In case 1, the fixed charge, i, is placed at the center of a mesh cell and the moved charge, j, is placed along a line through the center of the cell. In case 2, the fixed charge is placed at a mesh point and the moved charge is placed along the diagonal through mesh points to a corner of the mesh. In case 3, the fixed charge is again placed at a mesh point and the moved charge is placed along a mesh line. The point of this comparison is to note the difference in the mesh forces for each case. In particular, the third case results in a greater difference in the mesh force with that produced by the Coulomb force law than in the first two cases due to the reduced spreading of the charge in charge association and the sharply peaked potential which occurs at the location of the charges.

In addition to the issue of double counting the short-range force, there is clearly an issue of the orientation of the charge to the mesh and the effects of charge association and differencing to find the field. We must, therefore, consider a general transition error between long- and short-range domains and attempt to minimize it. The mesh force is determined in this work by a second-order cloud-in-cell (CIC) charge association and a second-order centered finite difference approximation for the potential derivative. The mesh-orientation component of the transition error may be reduced by adopting the third-order triangularly shaped cloud (TSC) charge association scheme over the CIC scheme [8] and higher order forms for the potential derivative, but short of solving the Poisson subproblem for each particular charge orientation, the transition error is impossible to eliminate fully. The result for the force law in Fig. 3 shows that the shape density approach effectively smoothes the force magnitude in the transition region and at least the double-counting component of the transition error is much reduced.

In Fig. 4, the force diagram is recalculated for a nonuniform rectilinear mesh $(41 \times 41 \times 41)$ where the mesh spacing is reduced in the center of the mesh to a 5 nm (along x), 10 nm (along y) and 20 nm (along z). In this case, the radius of the short-range domain in the mesh center is found using the procedure in Section IV as $r_{sr} = 2 \cdot 20$ nm $= 40$ nm. A charge, i, is fixed in the center of a mesh cell, while the moved charge, j, is placed along the lines down the center of the cells in each coordinate direction (as in case 1 for the uniform mesh). In Fig. 4, the mesh forces can be seen to peak at increasing radii for x, y, and z, where the peaks occur roughly at the mesh spacing. Despite the variation in the mesh forces, the modified shape density short-range correction produces a reasonably accurate estimate for the Coulomb force in all orientations as expected. An advantage of using a modified cutoff radius as done in this approach is that the extent of the short-range domain automatically adapts to variations in the mesh size. Such variations are common for rectilinear meshes employed in device simulation. It should also be noted that the improved accuracy in the corrected total forces in Fig. 4 as compared to those in Fig. 3 results, in part, from the consideration of only the lower-error centered orientation (case 1 in Fig. 3) and, in part, from the fact that the mesh is nonuniform and of higher resolution in the region tested compared to the uniform case.

IV. P3M-EMC Method

Considering now the more general problem of semiconductor transport simulation, we combine the extended P3M algorithm given above with the standard ensemble Monte Carlo (EMC) method. The combined P3M-EMC method (see Fig. 5) is a variation of the standard EMC method using a P3M to evaluate the c-i and c-c forces. Along with the particle-mesh solution for the electrostatic potential, the force sum is found for each

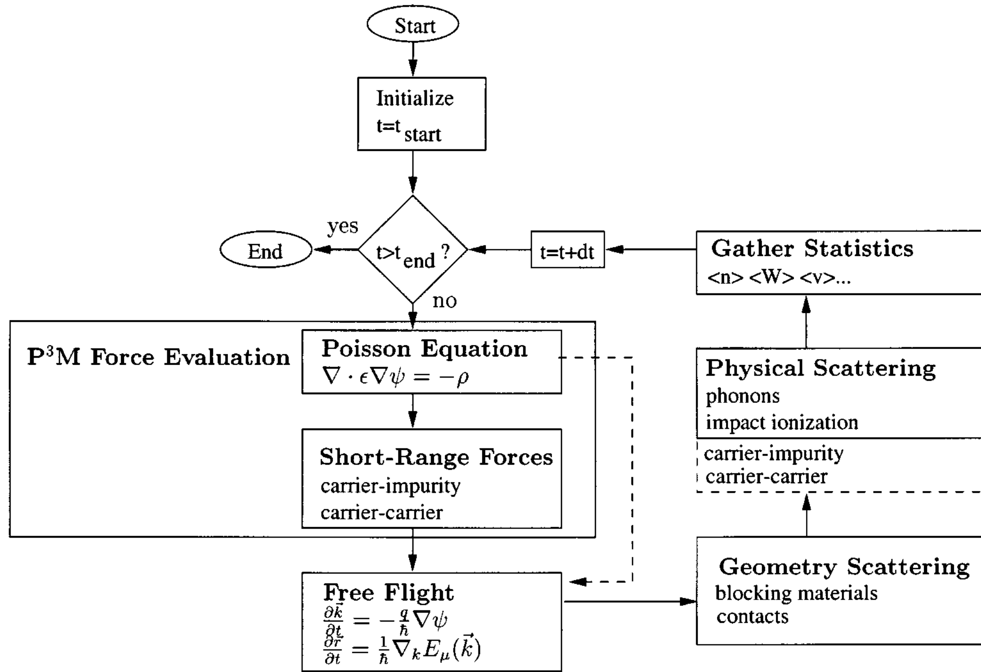

Fig. 5. Flowchart of the P3M-EMC method where bounding box denotes the P3M force evaluation and dashed lines revert to the standard EMC method.

particle within the cutoff radius and is added to the particle-mesh force while the c-i and c-c scattering rates used in continuum methods are omitted. Scattering by phonons, impact ionization, and blocking materials as well as device contacts and carrier dynamics are treated in the standard way by the EMC method.

A. Implementation Details

The P3M-EMC method was implemented in this work by solving the 3-D Poisson equation using the conjugate gradient method for nonuniform rectilinear meshes with arbitrary boundary conditions [12]. In all Monte Carlo simulations where the bias fields are low, accurate modeling of the low-energy band structure is important. In this work for Si, high accuracy of the band structure is achieved by using nonparabolic analytic band structure below 0.1 eV and empirical pseudopotential full band structure above it [13], [14]. In regions where the bias fields are low and the doping levels are low $(N_d \leq 10^{17}\ \mathrm{cm}^{-3})$, electron-phonon scattering effects are important. The electron-phonon scattering models used in this work are analytic rates based on nonparabolic analytic band structure for intervalley acoustic, f- and g-type X-X intervalley and X-L intervalley mechanisms with energies and deformation potentials as given by [15]. Also included is Cartier's model for impact ionization [16]. Above 1.0 eV, the rates are scaled by the density of states [17].

B. Considerations for Plasma Oscillations

Within the realm of classical physics, plasma oscillations are potential or particle density fluctuations which result from the correlated movement of charged particles with respect to a self-consistent field. As particles move and create voids, the self-consistent field forces particles into the voids [18]. As particles react to the field and approach points where the net force is zero, they may continue their motion if their kinetic energy is nonzero and proceed to oscillate.

Using the P3M algorithm for the treatment of short-range c-i and c-c interactions is economically advantageous to, but in principle equivalent to, using a fine Poisson mesh. In regard to 2-D EMC simulations using c-i and c-c scattering rates, it has been suggested [18], [19] that the resolution of Poisson meshes should be limited to the extrinsic Debye length. While this restriction is necessary in such a scheme to avoid double counting of the short-range forces with the c-i and c-c scattering rates, it introduces a significant limitation on the flexibility of mesh design [9] and is not an issue in the P3M-EMC method since Coulombic scattering rates are not used in this method.

A further limitation on the resolution of Poisson meshes used in 2-D EMC simulations has been explained [18], [19] as that required to enforce Landau damping, where Landau damping is the process which transfers the energy contained in a plasma oscillation to single particle(s). The references above explain that limiting mesh resolution to the critical damping wavelength insures that oscillations with wavelengths shorter than the critical wavelength are attenuated. We support the contention made in [20] and [21], that Landau damping is automatically accounted for in self-consistent particle-Poisson simulations. In this regard, we believe that no limitation on the mesh density or application of short-range methods is required when using a realistic carrier distribution as employed in the P3M-EMC method.

The remaining requirement to accurate modeling of plasma oscillations is on the time step of the synchronous ensemble. The Nyquist theorem calls for updating the field at a time interval of no more than $0.5\omega_p^{-1}$ to avoid undersampling the plasma

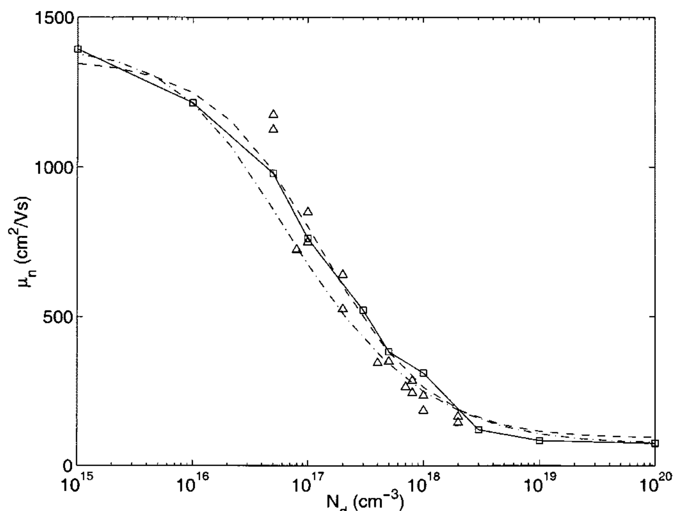

Fig. 6. Electron mobility versus donor doping where the dashed line and dot-dashed lines are best fits of experimental data from Baccarani and Ostoia [23] and Sharfetter and Gummel [23], the triangles are calculations by Gross *et al.* [3], and squares with solid line are done using the P3M-EMC method.

modes [15]. For the n-type resistors considered below, where $n = N_d^+ + p \cong N_d^+$, the inverse plasma frequency may be approximated as [18]

$$w_p^{-1} \cong \sqrt{(\epsilon m_c)/(e^2 n)}. \tag{9}$$

Here, m_c is the conductivity mass and for (100) silicon is given by $m_c = 3(2/m_t + 1/m_l)^{-1}$ with $m_l = 0.916 m_o$ and $m_t = 0.190 m_o$ [22]. For $N_d^+ < 10^{20}\ \mathrm{cm}^{-3}$ as considered below, the time interval called for by the Nyquist theorem is $0.5\omega_p^{-1} = 1.54$ fs. In order to satisfy this limit, a time step of 1 fs is used in our simulations.

C. Simulation Results for Bulk Mobility

An essential validation test for short-range Coulomb models in semiconductors is the simulation of low-field mobilities [5]. In order to make a direct comparison with existing results, we adopt a test case similar to that found in [3]. The test device is n-type bulk resistor with size chosen to maintain roughly 34 000 donors. The resistor is treated with a uniform $(41 \times 41 \times 41)$ mesh and results were obtained at 300K.

A uniform external field of $E^{ext} = 1$ kV/cm was used in the $\langle 100 \rangle$ direction with continuous particle boundary conditions and charge-neutral mesh boundary conditions. Since the field is within the linear region of the velocity-field characteristic [24], the electron mobility was approximated as $\mu_n \cong v_{\mathrm{drift}}/E_{ext}$, where v_{drift} is the ensemble average drift velocity. The drift velocity was averaged over 10 000 fs at an interval length of 100 fs and discarding a 2500 fs initial transient. The results in Fig. 6 indicate that the P3M-EMC method with a modified shape density correction compares well with the best-fit experimental results [23] and the related numerical approach in [3]. It should be noted that the approximations employed in c-i and c-c scattering rates have also been compared with experimental data in [25]. We feel, however, that the 3-D granular approaches exemplified by the P3M-EMC method have an advantage over short-range scattering rate approaches in that short- and long-range interactions can be treated in a unified way and that such methods are consistent in both bulk and granular conditions.

V. Conclusion

The P3M algorithm has been modified for application of nonuniform rectilinear meshes and arbitrary boundary conditions and combined with the EMC method as the P3M-EMC method. The P3M-EMC method replaces the standard treatment of c-i and c-c interactions with scattering rates, as used in two dimensions, with an explicit calculation of interparticle forces and scattering effects in three dimensions. Results indicate that the method can accurately reproduce Coulomb's law and mobility-doping characteristic in silicon while maintaining an approach that is capable of simulating nonuniform and boundary-affected devices such as a MOSFET. Work probing granular effects in an ultra-small MOSFET's using the P3M-EMC method is in progress.

The high degree of accuracy of the P3M-EMC method in reproducing experimental mobility data for silicon at room temperature indicates that c-i and c-c interactions in silicon can be adequately modeled by the semiclassical approach presented here. The use of a semiclassical approach may be questionable at much lower lattice temperatures because of the effects of quantum coherence on the transport, but we feel that the semiclassical approach should be applicable to deep-submicron Si devices at room temperature. Most important, the P3M-EMC method integrates 3-D granular treatment into the Monte Carlo method and continues the strongest merit of the method: the capability to model semiconductor devices with a high degree of physical accuracy and with a direct and verifiable approach.

Acknowledgment

The authors wish to thank D. K. Ferry for an advanced copy of reference [3].

References

[1] *The National Technology Roadmap For Semiconductors*, Semiconductor Industry Association, San Jose, CA, 1997.
[2] A. Asenov, "Random dopant induced threshold voltage lowering and fluctuations in sub-0.1 μm MOSFET's: A 3-D 'atomistic' simulation study," *IEEE Trans. Electron Devices*, vol. 45, pp. 2505–2513, 1998.
[3] W. J. Gross, D. Vasileska, and D. K. Ferry, "A novel approach for introducing the electron-electron and electron-impurity interactions in particle-based simulations," *IEEE Electron Device Lett.*, vol. 20, pp. 463–465, 1999.
[4] S. E. Laux and M. V. Fischetti, "Transport models for advanced device simulation—Truth or consequences?," in *Proc. 1995 BCTM*, Oct. 1995, pp. 27–34.
[5] R. P. Joshi and D. K. Ferry, "Effect of multi-ion screening on the electronic transport in doped semiconductors: A molecular-dynamics analysis," *Phys. Rev. B*, vol. 43, pp. 9734–9739, 1991.
[6] D. Vasileska, W. J. Gross, and D. K. Ferry, "Modeling of deep-submicrometer MOSFET's: Random impurity effects, threshold voltage shifts and gate capacitance attenuation," in *Ext. Abst. 1998 6th Int. Workshop on Computational Electronics*, Osaka, Japan, Oct. 19–21, 1998.
[7] P. Menziani, F. Rossi, and C. Jacoboni, "Impurity scattering in quantum transport simulation," *Solid-State Electron.*, vol. 32, pp. 1807–1811, 1989.
[8] R. W. Hockney and J. W. Eastwood, *Computer Simulation Using Particles*. New York, NY: McGraw-Hill, 1981.

[9] A. Pacelli, "Transport phenomena and hot electron effects in scaled MOSFET devices," Ph.D. dissertation, Polytech. Inst. Milan, Milan, Italy, 1997.
[10] R. J. Splinter, "A nested grid particle-mesh code for high resolution simulations of gravitational instability in cosmology," *Month. Notices R. Astronom. Soc.*, vol. 281, pp. 281–293, 1996.
[11] H. M. P. Couchman, "Mesh-refined P3M: A fast adaptive N-body algorithm," *Astrophys. J. Lett.*, vol. 368, pp. 23–26, 1991.
[12] A. Trellakis, A. T. Galick, A. Pacelli, and U. Ravaioli, "Iteration scheme for the solution of two-dimensional Schrödinger–Poisson equations in quantum structures," *J. Appl. Phys.*, vol. 81, pp. 7880–7884, 1997.
[13] M. L. Cohen and T. K. Bergstresser, "Band structures and pseudopotential form factors for fourteen semiconductors of the diamond and zine-blende structures," *Phys. Rev.*, vol. 141, pp. 789–796, 1996.
[14] J. R. Chelikowsky and M. L. Cohen, "Nonlocal pseudopotential calculations for the electronic structure of eleven diamond and zinc-blende semiconductors," *Phys. Rev.*, vol. 14, pp. 566–582, 1976.
[15] M. V. Fischetti and S. E. Laux, "Monte Carlo study of electron transport in silicon inversion layers," *Phys. Rev. B*, vol. 48, pp. 2244–2274, 1993.
[16] E. Cartier, M. V. Fischetti, E. A. Eklund, and F. R. Feely, "Impact ionization in silicon," *Appl. Phys. Lett.*, vol. 62, pp. 3339–3341, 1993.
[17] J. Y. Tang and K. Hess, "Theory of hot electron emission from silicon into silicon dioxide," *J. Appl. Phys.*, vol. 54, pp. 5145–5151, 1983.
[18] *Damocles User's Guide*, IBM Corp., 1996.
[19] M. V. Fischetti and S. E. Laux, "Monte Carlo analysis of electron transport in small semiconductor devices including band-structure and space-charge effects," *Phys. Rev. B*, vol. 38, pp. 9721–9745, 1988.
[20] P. Degond and F. Guyot-Delaurens, "Particle simulations of the semiconductor boltzmann equation for one-dimensional inhomogeneous structures," *J. Comput. Phys.*, vol. 90, pp. 65–97, 1990.
[21] M. V. Fischetti, S. E. Laux, and E. Crabbe, "Understanding hot-electron transport in silicon device: Is there a shortcut?," *J. Appl. Phys.*, vol. 78, pp. 1058–1087, 1995.
[22] S. M. Sze, *Physics of Semiconductor Devices*. New York, NY: Wiley, 1981.
[23] C. Jacoboni, C. Canali, G. Ottaviani, and A. Alberigi-Quaranta, "A review of some charge transport properties of silicon," *Solid-State Electronics*, vol. 20, pp. 77–89, 1977.
[24] R. S. Muller and T. I. Kamins, *Device Electronics for Integrated Circuits*. New York, NY: Wiley, 1986.
[25] M. V. Fischetti, "Effect of electron-plasmon interaction on the electron mobility in silicon," *Phys. Rev. B*, vol. 44, pp. 5527–5534, 1991.

Carl J. Wordelman (M'99) received the B.S. degree in physics and electrical engineering and the M.S. degree in electrical and computer engineering from the University of Illinois, Urbana–Champaign, in 1992 and 1995, respectively. He is currently pursuing the Ph.D. degree iin electrical and computer engineering at the University of Illinois, Ubrana–Champaign.

From 1996 to 1999, he was a member of the Plasma Physics Applications Group, Los Alamos National Laboratory, Los Alamos, NM. His research interests include the application of statistical enhancement, meshless methods, and molecular dynamics to Monte Carlo simulation of electron devices.

Umberto Ravaioli (SM'93) received the Laurea degree in electronics engineering in 1980 and the Laurea degree . in physics in 1982, both from the University of Bologna, Italy, and the Ph.D. degree in electrical engineering from Arizona State University, Tempe, in 1986.

He joined the Department of Electrical and Computer Engineering, University of Illinois, Urbana–Champaign, in 1986, where he is now a Professor. His research interests are in the areas of Monte Carlo device simulation, nanoelectronics, quantum transport, and supercomputation.